J. Phys. B: At. Mol. Opt. Phys. **41** (2008) 085403 (8pp) doi:10.1088/0953-4075/41/8/085403

Light switching at low light level based on changes in light polarization

Xudong Yang, Shujing Li, Xuemin Cao and Hai Wang

The State Key Laboratory of Quantum Optics and Quantum Optics Devices, Institute of Opto-Electronics, Shanxi University, Taiyuan 030006, People's Republic of China

E-mail: wanghai@sxu.edu.cn

Received 9 October 2007, in final form 14 February 2008
Published 7 April 2008
Online at stacks.iop.org/JPhysB/41/085403

Abstract

We studied the polarization spectroscopy of a linearly-polarized optical (probe) field in a multi-Zeeman-sublevel atomic system of the ^{87}Rb D1 line. The polarization spectroscopy signals of the probe light result from the changes in its polarization, which are caused by a left-circularly polarized pumping beam. A theoretical analysis involving multiple Zeeman sublevels is presented and the results are in qualitative agreement with the experimental observations. Based on this phenomenon, we demonstrated a light switch at low light level ($\sim$68 photons per $\lambda^2/2\pi$) with a switching efficiency of $\sim$3%.

(Some figures in this article are in colour only in the electronic version)

In the past 30 years, the polarization spectroscopy of a linearly-polarized laser beam caused by another laser beam has been extensively studied [1–7]. By letting a strong circularly polarized pumping beam counter-propagate through an atomic medium, Wieman *et al* observed Doppler-free laser polarization spectroscopy in an absorbing hydrogen gas via changes in light polarization [1]. They found that the signal-to-background ratio of the polarization spectroscopy could greatly surpass that of saturated absorption in the experiment. Later, several experimental and theoretical studies were presented [2–7]. Hughes's group experimentally studied the polarization spectroscopy of a closed atomic transition in the D2 line of ^{85}Rb [2], and later they made a theoretical analysis of their experimental results [3]. Other schemes to achieve the optical polarization rotation controlled by another stronger laser beam based on atomic coherence in multi-level electromagnetically induced transparency (EIT) systems were also studied [8–10].

All-optical switching can find important applications in the optical information processing [11]. Recently, a great deal of attention has been paid to realize all-optical switching at low light level [12–15], since it could be applied in optical quantum information processing. All-optical switching based on EIT in cold atoms has been reported by several groups [13–15]; the best result was achieved at a control energy density of $\sim 10^{-5}$ photons per atomic cross section $\lambda^2/2\pi$. There is also a study on all-optical switching based on a transverse optical pattern, with the reported lowest control energy density of 3×10^{-3} photons per $\lambda^2/2\pi$ [12].

In this paper, we studied the optical polarization spectroscopy of a linearly-polarized weak (probe) light beam controlled by a circularly polarized pumping beam in Rb vapour. In contrast to the work on the polarization spectroscopy reported in [2], the present work is more interested in an open two-level system of the ^{87}Rb D1 line. The polarization spectroscopy signal results from changes in the polarization of the probe beam and can be well explained by a simple theoretical model which involves the multi-Zeeman-sublevel system. Based on this phenomenon, we demonstrated a light switch at a low light level ($\sim$68 photons per $\lambda^2/2\pi$).

The experiment was performed in a multi-Zeeman-sublevel Rb atomic system, as shown in figure 1. We choose $5P_{1/2}$, $F' = 1$ to be the excited state $|c\rangle$, $5S_{1/2}$, $F = 2$ to be the ground state $|a\rangle$. The transition frequency from atomic levels $|a\rangle$ to $|c\rangle$ is denoted as ω_{ac}. The Zeeman sublevels of $5S_{1/2}$, $F = 2$ are denoted as $|a_i\rangle$ ($i = 1$–5 for $m = -2, -1, 0, +1, +2$), of $5P_{1/2}$, $F' = 1$ as $|c_k\rangle$ ($k = 1$–3 for $m = -1, 0, +1$), respectively. We choose the pumping field (with frequency ω_c) to be a left-circularly polarized (σ^-) beam driving levels $|a_{i+2}\rangle$ to $|c_i\rangle$ ($i = 1, 2, 3$) transitions. The linearly-polarized probe beam (with frequency ω_p) includes left-circularly polarized (σ^-) and right-circularly polarized (σ^+) components, which are near resonant with transition between levels $|a\rangle$ and $|c\rangle$. The frequency detunings of the probe and pumping laser beams

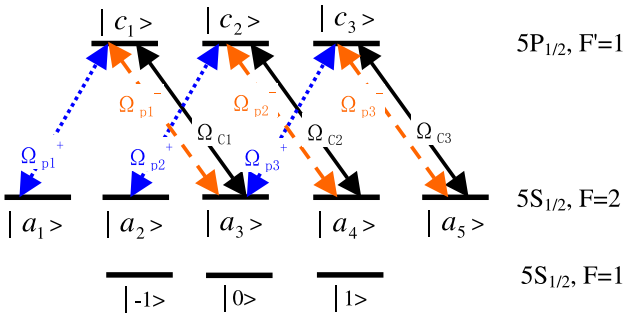

Figure 1. Relevant atomic energy level diagram of the D1 line in the ^{87}Rb atom. Solid line: transition for the left-circularly polarized pumping beam ; dotted line: transition for the right-circularly polarized probe beam; dashed line: transition for the left-circularly polarized probe beam.

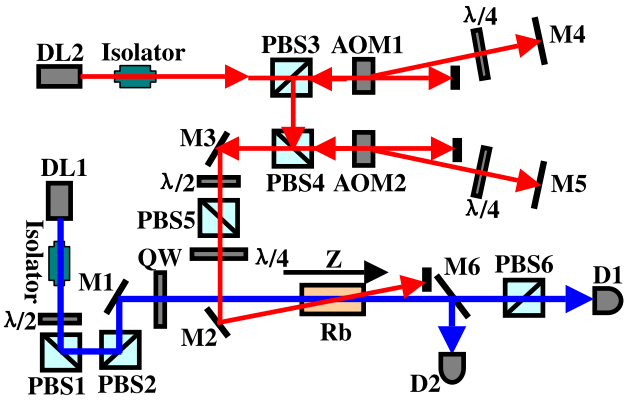

Figure 2. Experimental set-up. DL1 and DL2: diode lasers; PBS1-PBS6: polarization beam splitters; AOM1-AOM2: acousto-optical modulator; $\lambda/2$ and $\lambda/4$: half-wave and quarter-wave plates; M1–M6: mirrors with high reflectivity (where, M6 can be flipped), D1-D2: photodetectors. QW: removable quarter-wave plate.

are $\Delta_p = \omega_p - \omega_{ac}$ and $\Delta_c = \omega_c - \omega_{ac}$, respectively. The σ^- polarized probe beam couples to levels $|a_{i+2}\rangle$ to $|c_i\rangle$ ($i = 1, 2, 3$) transitions and the σ^+ polarized probe beam couples to levels $|a_i\rangle$ to $|c_i\rangle$ ($i = 1, 2, 3$) transitions, respectively.

Figure 2 depicts the experimental set-up. DL1 (probe beam) and DL2 (pumping beam) are both frequency stabilized diode lasers (linewidth ∼1.5 MHz) with grating feedback. After going through the polarization beam splitters PBS1 and PBS2, the probe beam becomes linearly polarized in the *s*-direction. The pumping beam first passes through a polarized-beam-splitter PBS3, acousto-optical modulator AOM1, and a quarter-wave plate, and then is reflected back along the original direction by a mirror M4. We use the 1-order diffracted beam from AOM1, so the frequency of pumping beam is up-shifted by 400 MHz after it doubly passes through AOM1. The reflected pumping beam by PBS4 passes through another acousto-optical modulator AOM2 and a quarter-wave plate, and then is reflected back through them again. We use the −1-order diffracted beam from AOM2, so its frequency is down-shifted by 400 MHz, and then it regains original frequency (ω_{ac}). Then the pumping beam becomes left-circularly polarized after going through a polarization beam splitter PBS5 and a quarter-wave plate. In the experiment, by switching the AOM2 on and off in time sequence, we achieve pulses of the pumping beam and use it to control the transmission of probe beam. QW in the probe arm is a removable $\lambda/4$ wave plate. When we observed the saturation spectra for σ^- (σ^+) probe beams, we used it to change the s-polarized probe beam into a σ^- (σ^+) probe beam. When the linearly-polarized probe beam is needed in measuring the polarization spectroscopy, it is removed. The probe and pumping beams co-propagate through a Rb vapour cell. The atomic cell is 50 mm long and its temperature is stabilized to 65 °C. The ambient magnetic field in the cell is reduced to about 20–30 mG by magnetic shielding. The diameters of the probe and pumping beams are 1 mm and 1.5 mm at the cell centre, respectively. The pumping beam is aligned at a small angle (about 2°) from the probe beam and they overlap well inside the Rb cell. After the probe beam passes through the cell, a mirror M6 was used to reflect it into a detector D2, and thus the absorption spectrum of the probe can be measured. Also, M6 can be flipped and the probe beam will enter a crossed polarizer (polarization beam splitter cube) PBS6. The extinction ration T_p/T_s of the PBS6 is more than 100:1 (where, T_p and T_s are the transmission of the p- and s-polarized light, respectively). If the probe beam does not experience a change in its polarization in the Rb cell, it will be fully reflected by PBS6. If the probe beam experiences a change in its polarization in the Rb cell, part of the probe beam will transmit from the crossed polarizer PBS6 and a polarization spectroscopy signal will be detected.

In the experiment, the pumping beam is locked to the atomic transition frequency ω_{ac}(i.e. $\Delta_c = 0$), and the probe frequency is scanned around the atomic transition frequency ω_{ac}. We first choose the input pumping beam to be the σ^- polarized light, and the input probe beam to be the σ^- and σ^+ polarized light, respectively. The absorption spectra of σ^- and σ^+ components of the probe beam are recorded for a probe power of 10 μW and a pumping power of 15 μW, as shown in figures 3(a) and (b). Figure 3(a) shows that a diminished absorption dip with a linewidth of ∼19 MHz appears at the resonance $\Delta_p = \Delta_c = 0$. While figure 3(b) shows that an enhanced absorption peak with a linewidth of ∼20 MHz appears at the resonance $\Delta_p = \Delta_c = 0$.

We next build a simple theoretical model and make numerical calculations to explain the experimental results in figure 3. When the σ^- pumping laser is tuned to the atomic resonant frequency ω_{ac}, it will only interact resonantly with the σ^- transitions ($|a_3\rangle \rightarrow |c_1\rangle$, $|a_4\rangle \rightarrow |c_2\rangle$ and $|a_5\rangle \rightarrow |c_3\rangle$) of the atoms with velocity $V_z = 0$ (width $\delta V_z = \Gamma_z/k$ [16], where Γ_z is the line width caused by radiative broadening, k is the wavevector). Thus, the uniformity of the populations on the Zeeman sublevels ($|a_1\rangle$ to $|a_5\rangle$) of $5S_{1/2}$, F = 2 is broken; the populations on the states $|a_1\rangle$ and $|a_2\rangle$ will be more than that of the states $|a_4\rangle$ and $|a_5\rangle$. Such asymmetry in the populations of the Zeeman sublevels will result in changes in the absorption and dispersion for σ^- and σ^+ probe fields near resonance. We theoretically calculated the absorption spectra of the σ^- and σ^+ probe fields to further explain such phenomena. The total susceptibilities of the σ^- and σ^+ probe beams are

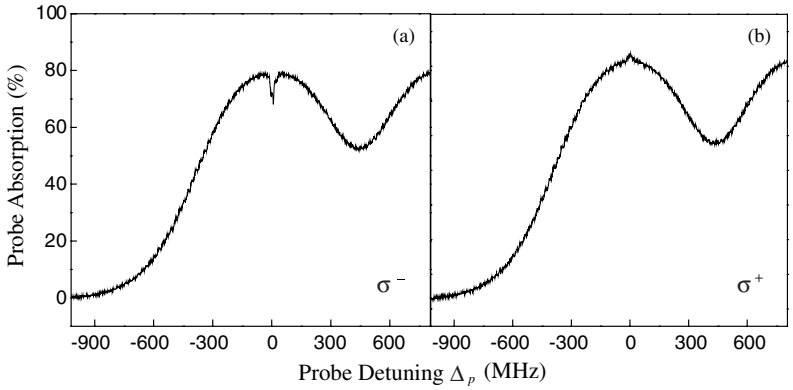

Figure 3. Measured probe absorption spectra: (a) and (b) are the results of σ^- and σ^+ probe beams for $\Delta_c = 0$. The power of the input left-circularly polarized pumping beam is 15 μW.

$$\chi^- = \chi_1^- + \chi_2^- + \chi_3^- \tag{1a}$$

$$\chi^+ = \chi_1^+ + \chi_2^+ + \chi_3^+, \tag{1b}$$

where χ_i^- is the susceptibility of the σ^- probe field coming from the transitions $|a_{i+2}\rangle$ to $|c_i\rangle$ ($i = 1$–3), and χ_i^+ is the susceptibility of the σ^+ probe field coming from the transitions $|a_i\rangle$ to $|c_i\rangle$ ($i = 1$–3). Under the stationary condition, the susceptibility $\chi_i^-(\chi_i^+)$ can be obtained by solving the density-matrix equations for the two-level atomic system and expressed as [17]

$$\chi_i^- = -\frac{N|\mu_{ai+2,ci}|^2}{\hbar\varepsilon_0}\frac{(\rho_{ai+2,ai+2} - \rho_{ci,ci})}{\Delta_p + \mathrm{i}\gamma_{\mathrm{ac}}} \tag{2a}$$

$$\chi_i^+ = -\frac{N|\mu_{ai,ci}|^2}{\hbar\varepsilon_0}\frac{(\rho_{ai,ai} - \rho_{ci,ci})}{\Delta_p + \mathrm{i}\gamma_{\mathrm{ac}}}, \tag{2b}$$

where $\gamma_{\mathrm{ac}} = \Gamma/2$, Γ is the spontaneous decay rates of the excited lever $|c\rangle$. N is the atomic density. $\mu_{ai,cj}$ is the dipole moment of the transition from Zeeman levels $|a_i\rangle$ to $|c_j\rangle$. $\rho_{ai,ai}(i = 1$–$5)$ and $\rho_{ci,ci}(i = 1$–$3)$ are the populations of states $|a_i\rangle$ and $|c_i\rangle$. The populations $\rho_{ai,ai}$ and $\rho_{ci,ci}$ are related to the intensities of the probe and pumping beams. When the probe beam is weak, the influence of the probe beam on the populations can be neglected and the populations can be calculated through density-matrix equations in the appendix, which involve the interaction of three frequency degenerate two-level atomic systems with the pumping field. Considering the frequency shifts due to the Doppler effect, the frequency detunings of pumping and probe fields will become $\Delta_c \to \Delta_c + \omega_c(v/c)$ and $\Delta_p \to \Delta_p + \omega_p(v/c)$, respectively (where v is the velocity of moving atoms), and thus χ_i^- and χ_i^+ can be rewritten as

$$\chi_i^- = \frac{\mathrm{i}|\mu_{ai+2,ci}|^2}{\hbar\varepsilon_0}\int_{-\infty}^{\infty}\frac{\rho_{ai+2,ai+2}(v) - \rho_{ci,ci}(v)}{-\mathrm{i}\Delta_p - \mathrm{i}\frac{v}{c}\omega_p + \gamma_{\mathrm{ac}}}N(v)\,\mathrm{d}v \tag{3a}$$

$$\chi_i^+ = \frac{\mathrm{i}|\mu_{ai,ci}|^2}{\hbar\varepsilon_0}\int_{-\infty}^{\infty}\frac{\rho_{ai,ai}(v) - \rho_{ci,ci}(v)}{-\mathrm{i}\Delta_p - \mathrm{i}\frac{v}{c}\omega_p + \gamma_{\mathrm{ac}}}N(v)\,\mathrm{d}v, \tag{3b}$$

where, $N(v) = \frac{N_{0,\mathrm{F2}}}{u\sqrt{\pi}}\mathrm{e}^{-v^2/u^2}$ is the Maxwellian velocity distribution, $N_{0,\mathrm{F2}} = \frac{5}{8}N_0$ is the total density of atoms staying in the energy level of $5S_{1/2}$, F = 2, N_0 is the atomic density of the vapour. The factor 5/8 is the ratio of the number of Zeeman sublevels in level F = 2 to the total number of Zeeman sublevels in levels F = 2 and F = 1. $u/\sqrt{2}$ is the root mean square atomic velocity and $\rho_{ai,ai}(v)$ and $\rho_{ci,ci}(v)$ are the populations and can be calculated through the equations in appendix. For example, we calculated the populations $\rho_{a1a1}(0) = 0.230\,36$, $\rho_{a2a2}(0) = 0.287\,64$, $\rho_{a3a3}(0) = 0.244\,32$, $\rho_{a4a4}(0) = 0.141\,04$, $\rho_{a5a5}(0) = 0.0771$ at $v = 0$ for $\Omega_c = 2\pi \times 3$ MHz (corresponding to the pump power of $P_c = 15$ μW), $\Gamma = 2\pi \times 5.8$ MHz, $\Gamma_a = 2\pi \times 0.05$ MHz.

Figure 4 plotted the calculated results through equations (1) and (3) with parameters $\gamma_{\mathrm{ac}} \approx 2\pi \times 3.5$ MHz and $N_0 = 6.56 \times 10^{16}$ m^{-3}. Figures 4(a) and (b) are the calculated absorption curves for σ^- and σ^+ probe fields, respectively. (c) and (d) are the dispersion curves for σ^- and σ^+ probe fields, respectively. The theoretical results clearly show that the enhanced absorption peak occurs at resonance in the σ^+ probe absorption curve and diminished absorption dip occurs at resonance in the σ^- probe absorption curve, which are in agreement with the experimental results as shown in figures 3(a) and (b). From figures 4(c) and (d), one can see that the anomalous ($\mathrm{d}n/\mathrm{d}\nu < 0$) and normal ($\mathrm{d}n/\mathrm{d}\nu > 0$) dispersion slope occur in the σ^- and σ^+ probe dispersion curves at resonance, respectively. Such a difference between the σ^+ and σ^- probe dispersion slopes near resonance will generate a significant difference between χ^+ and χ^-. We note that the atomic density ($N_0 = 6.56 \times 10^{16}$ m^{-3}) used in theoretical calculation are different from the experimental data $N_0 \sim 3.7 \times 10^{17}$ m^{-3} (corresponding to the atomic density at 65 °C). A main reason is that our two-level atoms is an open system; the population in the level F = 2 will decay into F = 1 [18] by spontaneous emission from the levels F′ = 1 to F = 1. Also the probe beam in our experiment is not weak, which will cause an influence on the populations in the level F = 2. These neglects will let us give a higher evaluation for the populations in the level F = 2.

We need to point out that an M-type system will be formed in such a multi-Zeeman-level atomic system when the σ^- and σ^+ components of the probe and pumping fields are coupled to

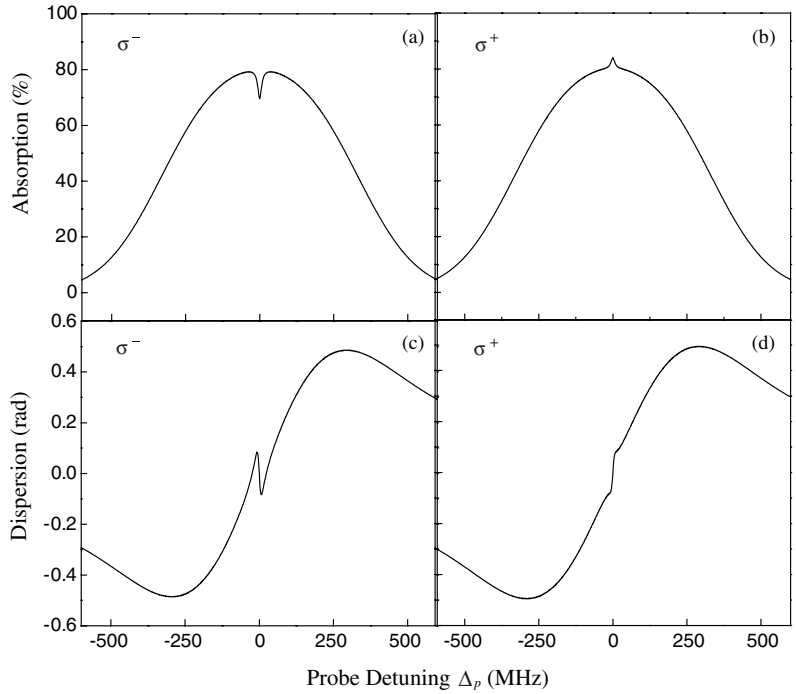

Figure 4. Theoretically calculated absorption and dispersion curves of the probe fields for $\Delta_c = 0$: (a) and (b) are the absorption curves for σ^- and σ^+ probe beams, respectively;. (c) and (d) are the dispersion curves for σ^- and σ^+ probe beams, respectively. The parameters used here are $\Omega_C \approx 2\pi \times 3$ MHz, $\gamma_{ac} \approx 2\pi \times 3.5$ MHz, $N_0 = 6.56 \times 10^{16}$ m^{-3}.

the corresponding transitions. Accompanying the saturation absorption due to optical pumping, atomic coherence will also be produced. The atomic coherence may generate an EIT [19] or coherent population trapping (CPT) [20] effect, which will change the light absorption and dispersion. But the intensities of both the probe and pump beams in our experiment are very low ($\sim$1 mW cm^{-2}), and then the CPT effect observed by us is very small. So, we neglect atomic coherence in the current work.

We also measured the absorption spectra of the σ^- and σ^+ probe beams, respectively, when a linearly-polarized pumping beam is injected into the Rb cell, the results are as shown in figures 5(a) and (b). One can see that the absorption spectrum of the σ^- probe beam (figure 5(a)) is almost the same as that of the σ^+ probe beam (figure 5(b)), which implies that the dispersion of the σ^- probe beam will be almost the same as that of the σ^+ probe beam. In this case, the polarization of the linearly-polarized probe beam will not be rotated when it passes through the atomic medium.

The difference between the absorption of σ^+ and σ^- probe beams, i.e. $\alpha_+ - \alpha_-$, induces a circular dichroism which will make the linearly-polarized probe beam elliptically polarized. While, the difference between the refractive indices of σ^+ and σ^- probe beams, i.e. $n_+ - n_-$, describes a circular birefringence which will rotate the axis of probe polarization [1]. So both differences $\alpha_+ - \alpha_-$ and $n_+ - n_-$ will induce changes in the polarization of the linearly-polarized probe beam. In our experimental arrangement, in the absence of changes in the polarization, the input linearly-polarized probe beam will be reflected by PBS6. If the input linearly-polarized probe beam experiences changes in its polarization in Rb cell, some of the probe beam will transmit from crossover polarizer PBS6 and be detected by D1. The probe intensity transmitted from the PBS6 can be written as [10]

$$I_D = I_{P,\mathrm{in}}\, \mathrm{e}^{-b}\left(\frac{1}{4}\,\mathrm{e}^{-\alpha_+ l} + \frac{1}{4}\,\mathrm{e}^{\alpha_- l} - \frac{\mathrm{e}^{-(\alpha_+ + \alpha_-)l/2}}{2}\cos\left[\frac{2\pi}{\lambda}(n_+ - n_-)l\right]\right)$$
$$= \frac{1}{2} I_T \left(\frac{1}{2}\,\mathrm{e}^{-\frac{\delta_\alpha l}{2}} + \frac{1}{2}\,\mathrm{e}^{\frac{\delta_\alpha l}{2}} - \cos\left[\frac{2\pi}{\lambda}(n_+ - n_-)l\right]\right), \qquad (4)$$

where $\delta_\alpha = \alpha_+ - \alpha_-$, $I_{P,\mathrm{in}}$ is the input intensity of the linearly-polarized probe beam (before cell), $I_T = I_{P,\mathrm{in}}\,\mathrm{e}^{-b-\alpha_0 l}$ is a average intensity of the probe beam transmitted from the Rb cell, i.e the average intensity before PBS6. $\alpha_0 = (\alpha_+ + \alpha_-)/2$ is an average absorption coefficient, l is the cell length. e^{-b} is the absorption due to the two windows. We calculated the transmitted probe intensity from the PBS6 as the function of Δ_p (polarization spectroscopy of the probe beam) for $\Delta_c = 0$ through equation (4), the result is shown in figure 6. One can see that a Lorentzian-type signal with a linewidth of $\sim$20 MHz appears, the maximum transmission (I_D/I_T) is achieved at $\Delta_p = 0$.

We next experimentally observed the transmitted probe beam from the PBS6 when the probe frequency was scanning across the atomic transition frequency for $\Delta_c = 0$. In the measurement, the power of the input linearly-polarized probe beam is kept at $P_{p,\mathrm{in}} = 10$ μW and the power of the pumping beam is kept at $P_{c,\mathrm{in}} = 15$ μW. Figures 7(a)

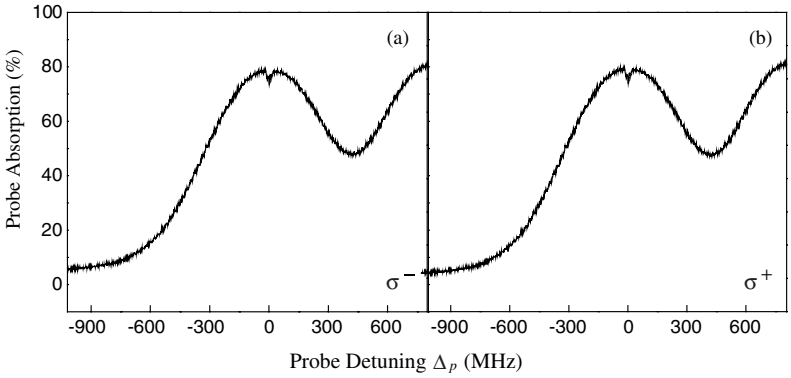

Figure 5. Measured absorption spectra of the probe beam with a linearly-polarized pumping beam: (a) and (b) are the results of the σ^- and σ^+polarized probe beams for a pumping power of 15 μW and $\Delta_c = 0$.

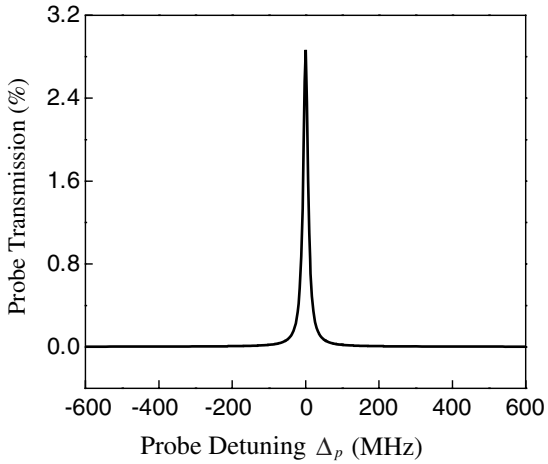

Figure 6. Theoretically calculated the probe transmission (I_D/I_T) from PBS6 as the function of Δ_P for $\Delta_c = 0$. The parameters used here are the same as in figure 4.

and (b) are the polarization spectroscopy signals with a left-circularly polarized pumping beam and a linearly-polarized pumping beam, respectively. One can see that an obviously transmitted probe signal with a linewidth of ∼20 MHz appears near resonance, the maximum transmission (I_D/I_T) achieved at resonance ($\Delta_p = 0$) is 3% when the pumping beam is left-circularly polarized. When we replace the left-circularly polarized pumping beam with the linearly-polarized pumping beam, the transmitted probe signal near resonance is almost zero. We also measured the transmission signal of the linearly-polarized probe beam without any pumping beam; the result is almost the same as that of figure 7(b), which implies that the polarization of the linearly-polarized probe beam will not be changed without the pumping beam.

The calculated and experimentally measured maximal probe transmissions (I_D/I_T) achieved at $\Delta_p = 0$ as a function of pumping power are plotted in figure 8. One can see that, with the increase of the power of the left-circularly polarized pumping beam, the maximal probe transmission becomes larger. The agreements between the theoretically calculated results (curve (b) in figure 8) and experimentally measured data (curve (a) in figure 8) are quite good.

We also calculated the dependence of the polarization rotation angle $\left(\Phi = \frac{\pi}{2\lambda}\,\mathrm{Re}(\chi^+ - \chi^-)l\right)$ on the probe frequency detuning Δ_p and found that significant polarization rotation

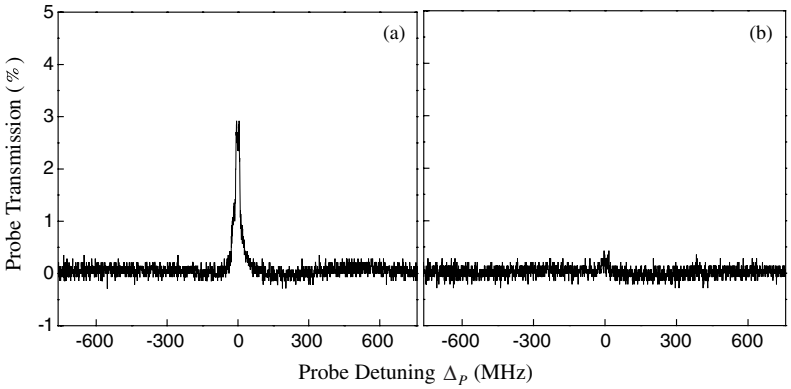

Figure 7. Experimentally measured probe polarization spectroscopy (I_D/I_T) for $\Delta_c = 0$: (a) the result for the left-circularly polarized pumping beam; (b) the result for the linearly-polarized pumping beam.

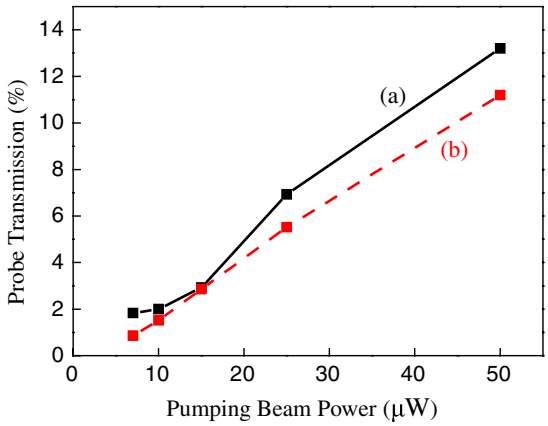

Figure 8. Dependence of the maximal probe transmission (I_D/I_T) achieved at $\Delta_p = 0$ on pumping powers for $\Delta_c = 0$. Curve (a) is the experimentally measured results. Curve (b) is the theoretically calculated results. The parameters used here are the same as in figure 4.

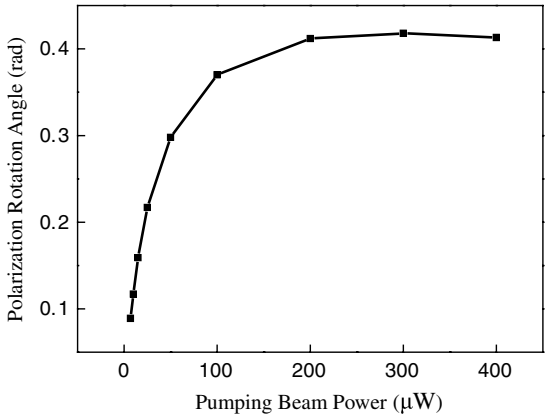

Figure 10. Theoretically calculated dependence of the maximum polarization rotation angle (at $\Delta_p = -8$ MHz) on the power of the left-circularly polarized pump beam for $\Delta_c = 0$. The parameters used here are the same as in figure 4.

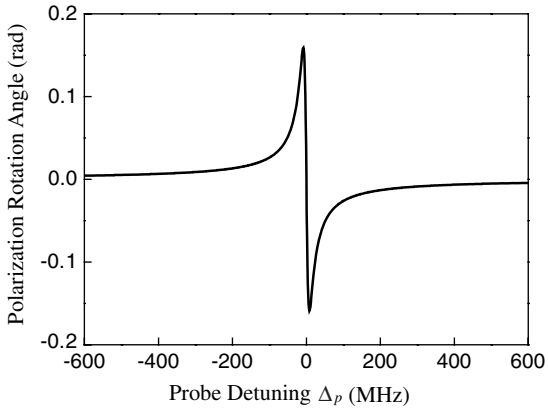

Figure 9. Theoretically calculated the dependence of the polarization rotation angle on the probe frequency detuning Δ_p for $\Delta_c = 0$. The parameters used here are the same as in figure 4.

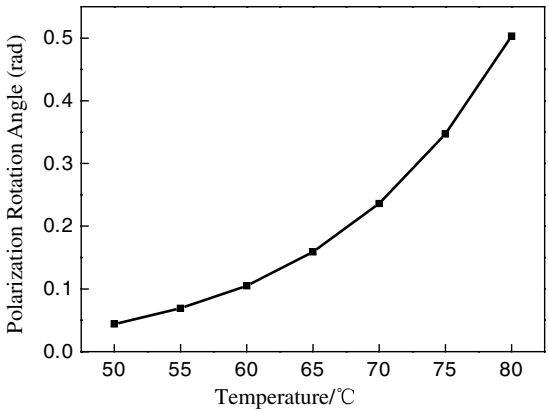

Figure 11. Theoretically calculated dependence of the maximum polarization rotation angle (at $\Delta_p = -8$ MHz) on the temperature for $\Delta_c = 0$. The parameters used here are the same as in figure 4.

occurred near resonance. As shown in figure 9, the two maximum polarization rotation angles corresponding to the two dispersionlike peaks achieve at $\Delta_p \approx \pm 8$ MHz. At $\Delta_p = 0$, the polarization rotation angle becomes zero. Combining with the measured result of polarization spectroscopy in figure 7, one can see that the maximum transmission achieved at resonance $\Delta_p = 0$ is only due to the contribution of the circular dichroism, while, at off resonance, the transmissions are caused by the combined contributions of the circular birefringence and dichroism. Figures 10 and 11 plotted the dependence of the maximum polarization rotation angle Φ_m achieved at $\Delta_p \approx -8$ MHz on the pump power and the temperature, respectively. One can see that Φ_m becomes larger with the increasing of the pumping power and the temperature, respectively.

The changes in polarization of probe beam controlled by a circularly polarized pumping can be harnessed to build up an all-optical switch. By using the acousto-optical modulator AOM2 to turn the left-circularly polarized pumping beam on and off (figure 12(b)), we observe switching behaviour of the probe beam near resonance $\Delta_p = \Delta_c = 0$, as shown in figure 12(a). One can see that the transmitted probe beam though PBS6 is also switched on and off when the pumping beam is turned on and off by the AOM2. The switching efficiency (I_D/I_T) is about 3% for a pumping power of 15 μW. Each pumping pulse (time duration $\sim$20 μs) include 1.2×10^9 photons, so the light switch is demonstrated at an energy per area of $\sim$68 photons per $\lambda^2/2\pi$ with a switching efficiency of $\sim$3%.

In summary, we studied the optical polarization spectroscopy of a linearly-polarized weak (probe) light beam controlled by a circularly polarized pumping beam in Rb vapour. The polarization spectroscopy signal results from changes in the polarization of the probe beam and can be well explained by a simple theoretical model which involves multi-Zeeman-sublevel atoms. Based on this phenomenon, we demonstrated a light switch at low light level (energy per area of $\sim$68 photons per $\lambda^2/2\pi$) with a switching efficiency of $\sim$3%. The experimental set-up is relatively simple since it

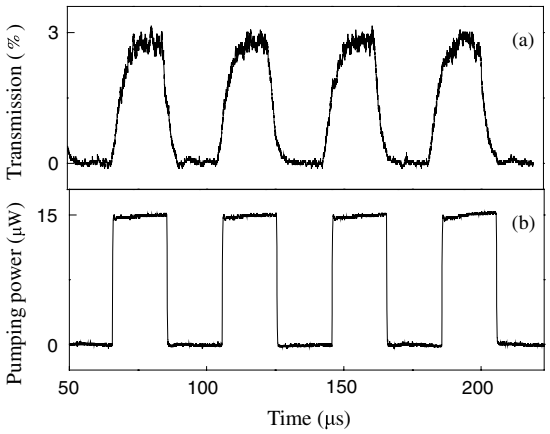

Figure 12. Optical switching signal of probe beam controlled by the left-circularly polarized pumping beam with a peak power of 15 μW. Top, the transmitted probe signal through PBS6. Bottom, modulated controlling power.

does not need the MOT system for trapping and cooling atoms and all-optical switching can be easily performed in such an atomic system. The control energy density of ∼68 photons per atomic cross section $\lambda^2/2\pi$ reaches low light level. We hope that such scheme of light switching can be extended in a solid or semi-conducting material and then find a practical application in all-optical information processing and quantum information processing.

Acknowledgments

We acknowledge funding support from the National Natural Science Foundation of China (#60325414, 6057805 10640420195 and RGC60518001), 973 Program (no 2006CB921103) and NSF of Shanxi Province (no 2007011004).

Appendix

The following equations are the density-matrix equations which are used to describe the interaction of three two-level subsystems with the pumping field. After the Doppler effect is taken into account ($\Delta_c \rightarrow \Delta_c + \omega_c(v/c)$), the populations $\rho_{\alpha i,\beta j}(v)$ can be calculated.

$$\dot{\tilde{\rho}}_{a1a1} = -4\Gamma_a\rho_{a1a1} + \Gamma_a(\rho_{a2a2} + \rho_{a3a3} + \rho_{a4a4} + \rho_{a5a5}) + \frac{\Gamma}{3}\rho_{c1c1}$$

$$\dot{\tilde{\rho}}_{a2a2} = -4\Gamma_a\rho_{a2a2} + \Gamma_a(\rho_{a1a1} + \rho_{a3a3} + \rho_{a4a4} + \rho_{a5a5}) + \frac{\Gamma}{3}\rho_{c1c1} + \frac{\Gamma}{3}\rho_{c2c2}$$

$$\dot{\tilde{\rho}}_{a3a3} = \mathrm{i}\left(\frac{1}{2}\Omega_{c1}\rho_{c1a3} - \frac{1}{2}\Omega^*_{c1}\rho_{a3c1}\right) - 4\Gamma_a\rho_{a3a3} + \Gamma_a(\rho_{a1a1} + \rho_{a2a2} + \rho_{a4a4} + \rho_{a5a5}) + \frac{\Gamma}{3}\rho_{c1c1} + \frac{\Gamma}{3}\rho_{c2c2} + \frac{\Gamma}{3}\rho_{c3c3}$$

$$\dot{\tilde{\rho}}_{a4a4} = \mathrm{i}\left(\frac{1}{2}\Omega_{c2}\rho_{c2a4} - \frac{1}{2}\Omega^*_{c2}\rho_{a4c2}\right) - 4\Gamma_a\rho_{a4a4} + \Gamma_a(\rho_{a1a1} + \rho_{a2a2} + \rho_{a3a3} + \rho_{a5a5}) + \frac{\Gamma}{3}\rho_{c2c2} + \frac{\Gamma}{3}\rho_{c3c3}$$

$$\dot{\tilde{\rho}}_{a5a5} = \mathrm{i}\left(\frac{1}{2}\Omega_{c3}\rho_{c3a5} - \frac{1}{2}\Omega^*_{c3}\rho_{a5c3}\right) - 4\Gamma_a\rho_{a5a5} + \Gamma_a(\rho_{a1a1} + \rho_{a2a2} + \rho_{a3a3} + \rho_{a4a4}) + \frac{\Gamma}{3}\rho_{c3c3}$$

$$\dot{\tilde{\rho}}_{c1c1} = \mathrm{i}\left(\frac{1}{2}\Omega^*_{c1}\rho_{a3c1} - \frac{1}{2}\Omega_{c1}\rho_{c1a3}\right) - \Gamma\rho_{c1c1}$$

$$\dot{\tilde{\rho}}_{c2c2} = \mathrm{i}\left(\frac{1}{2}\Omega^*_{c2}\rho_{a4c2} - \frac{1}{2}\Omega_{c2}\rho_{c2a4}\right) - \Gamma\rho_{c2c2}$$

$$\dot{\tilde{\rho}}_{c3c3} = \mathrm{i}\left(\frac{1}{2}\Omega^*_{c3}\rho_{a5c3} - \frac{1}{2}\Omega_{c3}\rho_{c3a5}\right) - \Gamma\rho_{c3c3}$$

$$\dot{\tilde{\rho}}_{a3c1} = \mathrm{i}\left(\frac{1}{2}\Omega_{c1}\rho_{c1c1} - \frac{1}{2}\Omega_{c1}\rho_{a3a3} + \Delta_c\rho_{a3c1}\right) - \gamma_{\mathrm{ac}}\rho_{a3c1}$$

$$\dot{\tilde{\rho}}_{a4c2} = \mathrm{i}\left(\frac{1}{2}\Omega_{c2}\rho_{c2c2} - \frac{1}{2}\Omega_{c2}\rho_{a4a4} + \Delta_c\rho_{a4c2}\right) - \gamma_{\mathrm{ac}}\rho_{a4c2}$$

$$\dot{\tilde{\rho}}_{a5c3} = \mathrm{i}\left(\frac{1}{2}\Omega_{c3}\rho_{c3c3} - \frac{1}{2}\Omega_{c3}\rho_{a5a5} + \Delta_c\rho_{a5c3}\right) - \gamma_{\mathrm{ac}}\rho_{a5c3}$$

$$\dot{\tilde{\rho}}_{c1a3} = \mathrm{i}\left(\frac{1}{2}\Omega^*_{c1}\rho_{a3a3} - \frac{1}{2}\Omega^*_{c1}\rho_{c1c1} - \Delta_c\rho_{c1a3}\right) - \gamma_{\mathrm{ac}}\rho_{c1a3}$$

$$\dot{\tilde{\rho}}_{c2a4} = \mathrm{i}\left(\frac{1}{2}\Omega^*_{c2}\rho_{a4a4} - \frac{1}{2}\Omega^*_{c2}\rho_{c2c2} - \Delta_c\rho_{c2a4}\right) - \gamma_{\mathrm{ac}}\rho_{c2a4}$$

$$\dot{\tilde{\rho}}_{c3a5} = \mathrm{i}\left(\frac{1}{2}\Omega^*_{c3}\rho_{a5a5} - \frac{1}{2}\Omega^*_{c3}\rho_{c3c3} - \Delta_c\rho_{c3a5}\right) - \gamma_{\mathrm{ac}}\rho_{c3a5},$$

where the density-matrix elements $\rho_{\alpha i,\beta j} = \langle \alpha i|\hat{\rho}|\beta j\rangle$. α and β denote the levels a or c, and i,j stand for the subscripts of Zeeman sub-level. $\Omega_{ci} = -\mu_{ci,ai+2}E_c/\hbar$ ($i = 1, 2, 3$) are the Rabi frequencies of the pumping beam for various transitions among different Zeeman sub-level. Γ is the spontaneous decay rate of the excited level $|c\rangle$ and $\gamma_{\mathrm{ac}} = \Gamma/2$. Γ_a is the decay rate for the ground states due to atomic collisions.

References

[1] Wieman C and Hansch T W 1976 *Phys. Rev. Lett.* **36** 1170
[2] Pearman C P, Adams C S, Cox S G, Griffin P F, Smith D A and Hughes I G 2002 *J. Phys. B: At. Mol. Opt. Phys.* **35** 5141
[3] Harris M L, Adams C S, Cornish S L, McLeod I C, Tarleton E and Hughes I G 2006 *Phys. Rev.* A **73** 062509
[4] Agrawal G P 1984 *Phys. Rev.* A **29** 994
[5] Liu Z D, Bloch D and Ducloy M 1994 *Appl. Phys. Lett.* **65** 274
[6] Teets R E, Kowalski F V, Hill W T, Carlson N and Hansch T W 1977 Advances in laser spectroscopy I *Proc. Soc. Photo-Opt. Instrum. Eng.* **113** 80
[7] Entin V M, Ryabtsev I I, Boguslavsky A E and Brzhazovsky Yu V 2002 *Opt. Commun.* **207** 201
[8] Wielandy S and Gaeta A L 1998 *Phys. Rev. Lett.* **81** 3359
[9] Yoon T H, Park C Y and Park S J 2004 *Phys. Rev.* A **70** 061803
[10] Li S, Wang B, Yang X, Han Y, Wang H, Xiao M and Peng K 2006 *Phys. Rev.* A **74** 033821
[11] Brown A W and Xiao M 2005 *Opt. Lett.* **30** 699
[12] Dawes A M C, Illing L, Clark S M and Gauthier D J 2005 *Science* **308** 672
[13] Braje D A, Balic V, Yin G Y and Harris S E 2003 *Phys. Rev.* A **68** 041801

[14] Zhang J, Hernandez G and Zhu Y 2007 *Opt. Lett.* **32** 1317
[15] Chen Y F, Tsai Z H, Liu Y C and Yu I A 2005 *Opt. Lett.* **30** 3207
[16] Foot C J 2005 *Atomic Physics* (New York: Oxford University Press) p 156
[17] Boyd R W 1992 *Nonlinear Optics* (New York: Academic)
[18] Alzetta G, Cartaleva S, Dancheva Y, Andreeva Ch, Gozzini S, Botti L and Rossi A 2001 *J. Opt.* B **3** 181
[19] Li Y and Xiao M 1995 *Phys. Rev.* A **51** R2703
[20] Renzoni F, Maichen W, Windholz L and Arimondo E 1997 *Phys. Rev.* A **55** 3710